Journal of Controlled Release 332 (2021) 225–232

Contents lists available at ScienceDirect

Journal of Controlled Release

journal homepage: www.elsevier.com/locate/jconrel

# FRET imaging revealed that nanocrystals enhanced drug oral absorption by dissolution rather than endocytosis: A case study of coumarin 6

Guangshuai Zhang [a], Yunzhi Wang [a], Zuopeng Zhang [b], Zhonggui He [a], Yang Liu [b,*], Qiang Fu [a,*]

[a] Wuya College of Innovation, Shenyang Pharmaceutical University, No. 103, Wenhua Road, Shenyang 110016, China
[b] School of Pharmaceutical Engineering, Shenyang Pharmaceutical University, No. 103, Wenhua Road, Shenyang 110016, China

ARTICLE INFO

*Keywords:*
Drug nanocrystals
Dissolution
Oral absorption
*In vivo* trafficking
Endocytosis

ABSTRACT

Nanocrystals (NCs) exhibit potential in improving oral bioavailability for poorly water-soluble drugs. However, whether NCs improve oral absorption by quick dissolution or by endocytosis remains inconclusive because tracking of dissolved drugs and NCs particles cannot occur simultaneously. In this study, we aim to elucidate how NCs improve oral absorption by using coumarin 6 (C6), an aggregation-caused quenching fluorophore, and 2-((5-(4-(dip-tolylamino)phenyl)thiophen-2-yl)methylene)malononitrile (MeTTMN), an aggregation-induced emission fluorophore. C6 was used as a model drug to prepare NCs and MeTTMN was incorporated to construct fluorescence resonance energy transfer (FRET) pairs. Thus, the molecular absorption can be detected using the fluorescence signal of dissolved C6 and the NCs particles can be tracked simultaneously by monitoring FRET signals. The reliability of this tracking method was validated. Accordingly, *in vitro* dissolution, gastrointestinal traffic, and biodistribution studies were conducted. The results showed that dissolved C6 molecules were the main absorption mode of C6 NCs. Identification of such pathways bears considerable significance for the broad application of drug NCs in improving the druggability of insoluble drugs.

## 1. Introduction

Nanocrystals (NCs) have drawn wide interest because of their ability to effectively improve the bioavailability of drugs with poor water solubility [1]. However, the method by which NCs improve oral bioavailability remains undetermined, and two divergent viewpoints currently exist: the traditional view suggests that reduced particle sizes and improved solubility play decisive roles in improving bioavailability, whereas recent studies indicate that endocytosis as NCs primarily contribute to oral absorption [27],3]. The issue remains inconclusive because of deficiencies in tracking nanoparticles visually.

The aforementioned problem may be addressed by the rapid development of bioimaging. Owing to its simplicity of operation, high sensitivity, and high security, fluorescence tracking is the most widely used bioimaging technique in laboratories [4]. Fluorescence dyes can be classified into two classes by their photophysical properties: (a) aggregation-caused quenching (ACQ) fluorophores and (b) aggregation-induced emission (AIE) fluorophores [5,6]. ACQ fluorophores emit fluorescence in the dissolved state but are always quenched when they aggregate because of strong π–π interactions at high concentrations [7]. NCs can be tracked by dispersing the ACQ fluorophores they contain. Thus, translocation of NCs following intravenous administration is explored using an ACQ probe [8]. However, free dyes released from NCs interfere in tracking NCs [9]. By contrast, AIE fluorophores can be excited in an aggregated state but quenched in a molecular state [10]. Thus, tetraphenylethene (an AIE fluorophore) is used to explore the *in vivo* fate of paclitaxel NCs [11]. However, the fluorescence signal is reilluminated and produces interference when AIE fluorophores reprecipitate despite large Stokes shift, high luminosity, high photobleaching resistance, and excellent biocompatibility [12]. Thus, the released drug molecules and nanoparticles cannot be tracked concurrently by using a single probe.

Fluorescence resonance energy transfer (FRET) is the transfer of energy between two fluorophores (one as a donor and the other as an acceptor) and is used to detect the interaction of two labeled molecules in close proximity [13]. FRET was recently used in tracking NCs particles with a pair of ACQ fluorophores, and puerarin NCs were identified in the intestine and brain of zebrafish [14]. However, pseudosignals were emitted because the released ACQ pairs were reilluminated [15]. In addition, drug release from NCs cannot be monitored simultaneously.

To elucidate the method by which NCs improve oral absorption, coumarin 6 (C6), an ACQ fluorophore, was selected as a model drug, and

* Corresponding authors.
*E-mail addresses:* y.liu@syphu.edu.cn (Y. Liu), fuqiang@syphu.edu.cn (Q. Fu).

https://doi.org/10.1016/j.jconrel.2021.02.025
Received 1 October 2020; Received in revised form 16 January 2021; Accepted 22 February 2021
Available online 26 February 2021

C6 NCs were constructed. Free C6 could thus be detected using the ACQ signal. In addition, 2-((5-(4-(dip-tolylamino)phenyl)thiophen-2-yl) methylene)malononitrile (MeTTMN), an AIE fluorophore, was incorporated to construct FRET pairs with C6, and NCs particles were monitored simultaneously by monitoring the FRET pairs. The reliability of this tracking method was validated. Accordingly, *in vitro* dissolution, gastrointestinal traffic, and biodistribution studies were conducted. The results showed that dissolved C6 molecules were the main absorption mode of C6 NCs. This study provided insights into the oral absorption mechanism of drug NCs and elucidated the fate of NCs in the gastrointestinal tract and their drug performance *in vivo*.

## 2. Experimental section

### 2.1. Materials

Coumarin 6 (laser-grade), phosphate-buffered saline (PBS), 4% paraformaldehyde (PFA), and optimal cutting temperature (OCT) compound were purchased from Dalian Meilun Biotechnology Co., Ltd. (Dalian, Liaoning, China). Cremophor® EL and Pluronic F127 were purchased from BASF Co., Ltd. (Shanghai, China). Hank's balanced salt solution (HBSS) was supplied by Hyclone Laboratories, Inc. (Hyclone, USA). 4′,6-diamidino-2-phenylindole (DAPI) was purchased from Beyotime Biotechnology Co., Ltd. (Haimen, China). All other reagents and chemicals were of analytical grade.

### 2.2. Fluorescence characterization of C6 and MeTTMN

The fluorescence features of C6 and MeTTMN were examined by monitoring their fluorescence intensity in water/methanol solutions with different volumetric percentages at a fixed concentration of 2 μg/mL. For C6, the excitation wavelength ($E_x$) was set at 452 nm and the emission wavelength ($E_m$) at 566 nm. For MeTTMN, $E_x$ was set at 520 nm and $E_m$ at 664 nm. To evaluate the changes in fluorescence intensity, the relative fluorescence intensity (F) was calculated using the following equation:

$$F\ (\%) = \frac{F_x}{F_{max}} \times 100\%$$

where $F_x$ is the fluorescence intensity in the water/methanol solution (*x* %, *v/v*). For C6, $F_{max}$ is the fluorescence intensity in methanol. For MeTTMN, $F_{max}$ is the fluorescence intensity in water.

The samples were also observed using an IVIS Lumina III live imaging system (PerkinElmer, USA) and a YOKO-BA UV lamp (Wuhan Yaoke Technology Co., Ltd., China). Excitation and emission spectra were recorded using a Varioskan Flash multiplate reader (ThermoFisher, Finland).

### 2.3. Preparation and characterization of NCs

#### 2.3.1. Preparation of NCs

C6 NCs and MeTTMN NCs (M NCs) were prepared using the anti-solvent method. Up to 160 μL of the C6 methanol solution (0.03%, *w/v*) was injected into 5 mL of the Pluronic F127 aqueous solution (0.002%, *w/v*), which was kept in an ice bath, under ultrasound by using a SCIENTZ-IID ultrasonic homogenizer (Ningbo Scientz Biotechnology Co., Ltd., China). The input power was set at 400 W for 5 min, and intermit sonication was performed for 3 s at 2 s intervals. Similarly, C6/M NCs were prepared using the same processes, and MeTTMN was dissolved in the C6 methanol solution (0.03%, *w/v*) before precipitation. To remove the unembedded MeTTMN, the C6/M NCs were centrifuged at 21000*g* for 30 min and redispersed three times in 5 mL of the Pluronic F127 aqueous solution (0.002%, *w/v*). The energy transfer efficiency was used to evaluate the FRET efficiency and calculated using the equation below [16]:

$$\text{Energy transfer efficiency}\ (\%) = \left(1 - \frac{F_{DA}}{F_D}\right) \times 100\%$$

where $F_{DA}$ is the fluorescence intensity of the donor in the presence of the acceptor, and $F_D$ is the fluorescence intensity of the donor in the absence of the acceptor.

To achieve high FRET efficiency, the C6/M NCs were optimized (the amount of C6 was held constant) by varying the C6-to-MeTTMN molar ratio, and physical mixtures of C6 NCs and M NCs were set as controls.

The C6/M solution (C6/M Sol) was prepared by dissolving 1.25 mg of C6 in 1 mL of ethanol and Cremophor® EL cosolvent (1:1, *v/v*) and diluting to the working concentration before use. C6/M MCs were prepared by directly injecting 160 μL of the C6 methanol solution (0.03%, *w/v*) into 5 mL of the Pluronic F127 aqueous solution (0.002%, *w/v*).

#### 2.3.2. Sizes and zeta potentials

The particle sizes and zeta potentials of C6/M NCs and C6 NCs were characterized using a Zetasizer Nano ZS90 (Malvern Instruments Ltd., UK). All samples were measured in triplicate at a fixed angle of 90° at 25 °C.

#### 2.3.3. Morphology

To observe the morphology of C6/M NCs and C6 NCs, samples were dropped onto copper grids (Beijing Zhongjingkeyi Technology Co., Ltd., China) with a 200-mesh carbon membrane and dried in air. The grids were then observed using the H-7650 transmission electron microscopy (TEM) (Hitachi, Japan) operated at an acceleration voltage of 200 kV. The morphology of C6 NCs and C6/M NCs was also observed using the S-3400 N scanning electron microscopy (SEM) (Hitachi, Japan). The copper grids with samples were placed on a conducting resin and sputtered with gold under an inert environment of argon for observation.

#### 2.3.4. Crystallinity

The crystallinity of the NCs was evaluated using an X'pert Pro MPD X-ray diffractometer (PANalytical, Netherlands) with Cu-Kα radiation. The scan rate was 2°/min over a 2θ range of 3°–50°, and the step size was 0.03°.

#### 2.3.5. Fluorescence characterization of C6/M NCs

To evaluate the fluorescence properties of C6/M NCs, the emission spectra of C6/M NCs, C6 NCs, and MeTTMN were recorded using the multiplate reader at Ex = 452 nm. In addition, to prove the correlation between C6/M NCs and FRET phenomenon, about 0.5 mL of the C6/M NCs was added into 5.0 mL of the methanol/water binary system with incremental fractions of methanol, and the emission spectra of the samples were recorded immediately.

### 2.4. Method validation

#### 2.4.1. The linear correlation

For accurate quantification, the lower limit of quantification (LLOQ) and the linearity between NCs content and fluorescence signal were examined. For the LLOQ, free C6 and C6/M NCs were diluted with methanol and water, respectively. The samples were then measured using a multiplate reader until the fluorescence signal for the diluted sample was not significantly different ($p > 0.05$) from the diluent.

Furthermore, to test whether the FRET signal was proportional to the residual C6/M NCs, different ratios of methanol/water solution (5 mL) was used to dilute C6/M NCs (0.5 mL). The total C6 and dissolved NCs (filtered *via* a 100 nm membrane) were quantified by using the multiplate reader. Thus, the amount of residual C6/M NCs could be calculated. Then, the residual C6/M NCs percentage and the residual FRET signal intensity percentage were linearly fitted. More importantly, linear fitting was also performed in fasted-state simulated intestinal fluid

(FaSSIF) and fed-state simulated intestinal fluid (FeSSIF) to evaluate the accuracy of real-time tracking in the gastrointestinal tract.

#### 2.4.2. Reprecipitation studies

To determine whether the FRET signal could be reilluminated after supersaturation dissolution and precipitation, the C6/M NCs were dissolved in methanol, followed by dialysis in water by using a dialysis bag (cut-off molecular weight = 100 Da) for 12 h. After dialysis, the samples (reprecipitated C6/M NCs) were collected, and the emission spectrum was recorded at an $E_x$ of 452 nm. The C6/M NCs diluted 4-fold with water were set as the control.

#### 2.4.3. Mucus permeation

Sprague–Dawley (SD) rats (male, 220–250 g) were purchased from Shenyang Changsheng Animal Center, China. All animal experiments were approved by the Animal Ethics Committee of Shenyang Pharmaceutical University (Shenyang, China) and were conducted in accordance with the *Guidelines for the Care and Use of Laboratory Animals*.

To explore whether C6 and C6/M NCs could be tracked after passing through the mucus, the mucus diffusion was studied [17]. Prior to mucus diffusion, the dilution stability of C6 NCs and C6/M NCs were assessed to ensure the reliability. Both the diluted samples (diluted 4-fold with HBSS) and the undiluted controls were kept at 37 °C. The particle sizes and fluorescence intensity were then measured at intervals of 0, 0.5, 1, 2, 3, 5, 8, 12, and 24 h. To measure the fluorescence, $E_x$ was set to 452 nm. The FRET signals were collected at 664 nm and the donor signals at 566 nm. To evaluate the integrity of C6/M NCs, the FRET ratio was determined using the following equation [18]:

$$\text{FRET ratio} = F_A/(F_D + F_A)$$

where $F_A$ is the FRET signal intensity, and $F_D$ is the donor signal intensity.

For mucus diffusion, 100 μL of the intestinal mucus collected from rats was added to the apical side of Transwell® 3415 (Corning Costar, USA). Subsequently, 600 μL of HBSS was added into the basolateral side, and 300 μL of C6/M MCs, C6/M NCs, and C6/M Sol (2.5 μg/mL) was added to the apical side and maintained at 37 °C. At predetermined time points (0.25, 0.5, 1, and 2 h), 200 μL of the basolateral medium was withdrawn and refreshed with an equal volume of HBSS. The concentration of C6 in the basolateral side was determined. At the last time point, the residual basolateral medium was collected and observed using the TEM. In addition, the emission spectra of the basolateral medium were recorded at $E_x$ = 452 nm by using the multiplate reader.

#### 2.4.4. In situ intestinal absorption

To evaluate the reliability in tracking both the free C6 and C6/M NCs, in gastrointestinal microenvironment, *in situ* intestinal absorption studies were performed. Male SD rats were fasted overnight with free access to water before the experiments were conducted. The rats were anesthetized using chloral hydrate (500 mg/kg) *via* intraperitoneal injection, and midline laparotomy was conducted to expose segments (about 5 cm) of jejunum and ileum. 500 μL of C6/M MCs, C6/M NCs, and C6/M Sol (10 μg/mL) was then perfused into the intestines. The intestinal segments were removed after the rats were sacrificed 0.5, 1, and 2 h postperfusion. The intestinal segments were then washed with PBS, fixed with 4% PFA, and dehydrated in 30% sucrose. The samples were frozen with the OCT compound and sliced using a CM3050S cryostat (Leica Inc., Germany). The slices were then stained with DAPI and observed using an A1R confocal laser scanning microscope (CLSM) (Nikon, Japan).

### 2.5. In vitro dissolution

The dissolution test was carried out in a ZRS-8G dissolution apparatus (Tianda Tianfa Technology Co., Ltd., China). In detail, the dissolution medium (FaSSIF and FeSSIF) was 100 mL and paddle speed was 50 rpm. C6/M MCs, C6/M NCs, and the physical mixture of C6 NCs and M NCs (equivalent to 20.75 μg C6) were each placed into the dissolution medium, which was kept constant at 37 °C. Next, 2 mL of each sample was withdrawn at 5, 10, 20, 30, 45, 60, 120, and 240 min and immediately replaced with fresh dissolution medium. After filtering with 100 nm microporous filters, the samples were quantitatively analyzed using the multiplate reader.

### 2.6. Gastrointestinal traffic and biodistribution

To understand the oral absorption mechanism of NCs, the gastrointestinal traffic and biodistribution of the NCs were examined. Kunming mice (male, 18–22 g) were purchased from Shenyang Changsheng Animal Center, China. Three mice in each group (C6/M MCs, C6/M NCs, and C6/M Sol, 0.015 mg/kg) were euthanized at predetermined time intervals (0.05, 0.083, 0.25, 0.5, 1, 2, 4, 6, 8, 12, and 24 h) after single gavage dosing. The entire gastrointestinal tract, plasma, and main organs (heart, liver, spleen, lung, and kidney) were collected, and both the dissolved C6 and C6/M NCs particles were observed using the IVIS live imaging system ($E_x$ = 452 nm, $E_m$ = 566, 664 nm). In addition, the duodenum, jejunum, and ileum of gastrointestinal tracts were treated as described in 2.4.5. and colocalization of the dissolved C6 and C6/M NCs particles with enterocytes was achieved using the CLSM.

### 2.7. Statistical analysis

Data were statistically analyzed using SPSS (SPSS Inc., USA). One-way ANOVA was performed to determine whether a significant difference between groups was indicated. $p < 0.05$ was considered statistically significant.

## 3. Results and discussion

### 3.1. Fluorescence properties

The fluorescence properties of C6 and MeTTMN were evaluated by measuring the fluorescence intensity in water/methanol solutions with different volumetric percentages. As shown in Fig. 1A-B, both fluorophores showed water-dependent fluorescence intensity but exhibited different features. With an increase in water fraction, the fluorescence intensity of C6 decreased gradually, whereas that of MeTTMN increased. This occurrence could be attributed to the different aggregation states of C6 and MeTTMN: for the aggregated C6 molecules, the π-π stacking interactions among the planar π-conjugated frameworks induced a decrease in emission; for MeTTMN, the aggregation blocked the non-radiative path by inhibiting the intramolecular rotation and led to the increase in emission [19].

Spectral overlap is essential for FRET effects [13]. Thus, the fluorescence spectra of C6 and MeTTMN were recorded and presented in Fig. 1C. The emission spectrum of C6 and the excitation spectrum of MeTTMN overlapped between 475 and 650 nm, suggesting the occurrence of energy transfer from C6 to MeTTMN. Consequently, C6 and MeTTMN were used to construct an efficient FRET pair.

### 3.2. Preparation and characterization of NCs

The C6/M NCs were prepared using the antisolvent method, and the emission spectrum was recorded to identify the effects of FRET. Upon excitation at 452 nm, C6 exhibited an emission peak at 566 nm, and MeTTMN showed weak emission at 700 nm (Fig. 1D). However, after the embedment of MeTTMN, the C6/M NCs exhibited a strong emission peak at 700 nm upon excitation at 452 nm, indicating the successful transfer of energy from C6 to MeTTMN. Next, the C6-to-MeTTMN molar ratio was optimized to increase the FRET efficiency for semiquantitative determination. The C6/M NCs achieved the highest energy transfer

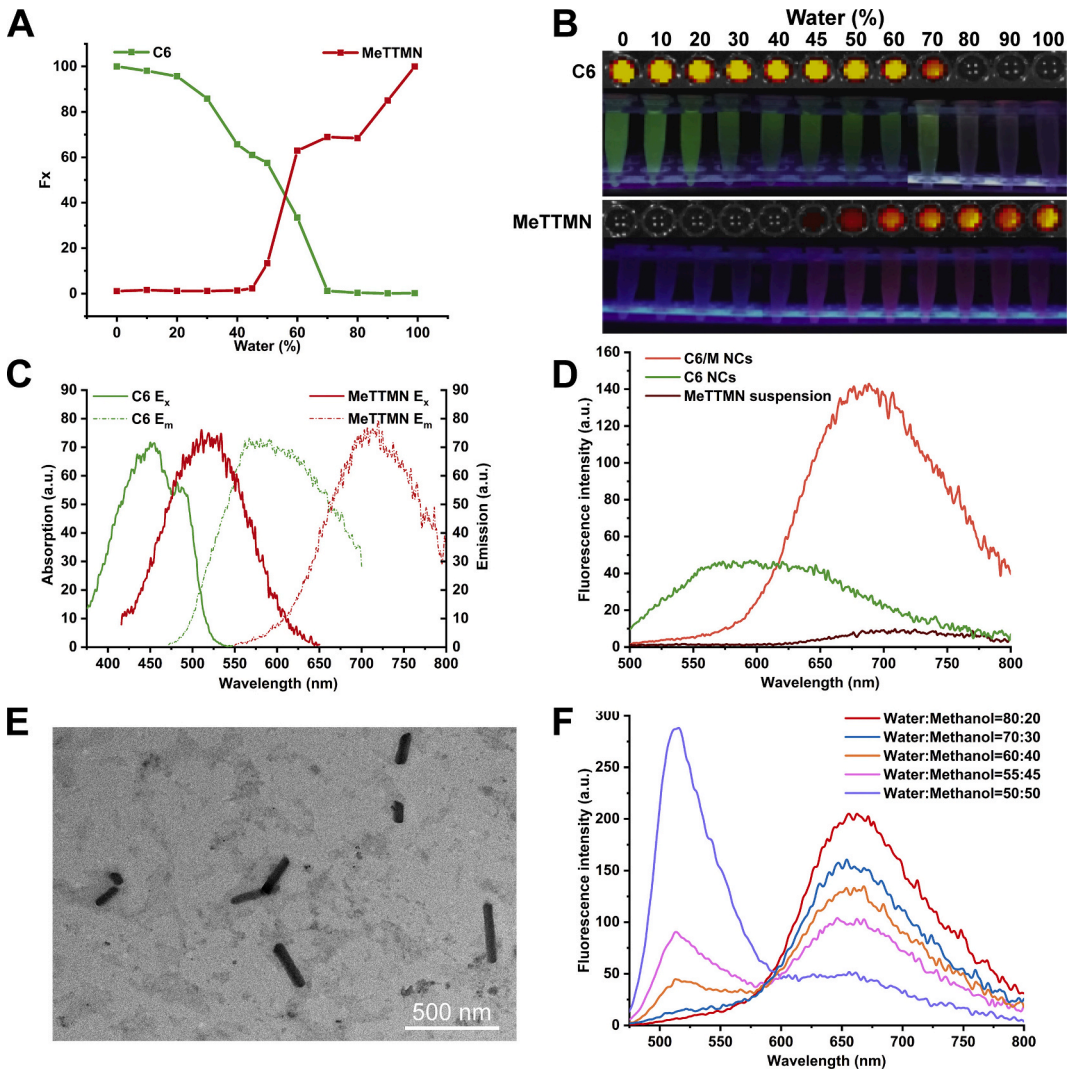


**Fig. 1.** (A) Fx, relative fluorescence intensity of C6 and MeTTMN in various water/methanol solutions. (B) Images of C6 and MeTTMN in various water/methanol solutions under IVIS and UV light. (C) Absorption and emission spectra of C6 and MeTTMN. (D) Emission spectra of C6/M NCs, C6 NCs, and MeTTMN suspension obtained upon excitation at 452 nm. (E) TEM images of C6/M NCs. (F) Emission spectra of C6/M NCs in different water/methanol (*v/v*) binary systems.

efficiency (84.68 ± 0.58%) when the C6-to-MeTTMN molar ratio was 10:3 (Fig. S1).

The physicochemical properties of the optimized C6/M NCs were evaluated. The mean particle sizes and zeta potentials of C6/M NCs were 252.57 ± 6.27 nm and − 8.04 ± 0.05 mV, which were similar to C6 NCs (Table 1). Both TEM and SEM images revealed that the C6/M NCs and C6 NCs were homogeneous and rod-shaped (Fig. 1E and Fig. S2). As shown in Fig. S3, the PXRD patterns showed that all characteristic peaks of C6 are detected in C6/M NCs, indicating the crystalline state. In summary, the C6/M NCs exhibited physicochemical properties similar to those of C6 NCs. Thus, the C6/M NCs could be used to reflect the *in vitro* and *in vivo* fate of the C6 NCs.

Subsequently, the photo-properties of the C6/M NCs were evaluated by dispersing the C6/M NCs in different methanol/water binary systems. As shown in Fig. 1F, with an increase in methanol content, the donor signal increases, while the FRET signal gradually decreases. The donor and FRET signals were related to the amounts of the dissolved C6 and NCs particles, respectively. Thus, any changes in the NCs particles could be tracked.

**Table 1**
The particle sizes, PDIs and zeta potentials of C6 NCs and C6/M NCs (mean ± SD, $n = 3$).

| Samples | Particle sizes (nm) | PDIs | Zeta potentials (mV) |
|---|---|---|---|
| C6 NCs | 228.92 ± 4.48 | 0.197 ± 0.029 | −11.41 ± 0.23 |
| C6/M NCs | 252.57 ± 6.27 | 0.223 ± 0.048 | −8.04 ± 0.05 |

### 3.3. Method validation

#### 3.3.1. LLOQ and linearity

Adequate sensitivity is necessary for tracking the fate of NCs. Thus, the LLOQ was studied by diluting free C6 and C6/M NCs with methanol and water, respectively. The LLOQ of free C6 and FRET for C6/M NCs were 0.1 and 2.5 ng/mL, respectively. Furthermore, to ensure the accurate tracking of the C6/M NCs, the linear correlations between the percentage of undissolved C6/M NCs and the fluorescence intensity of the FRET signals were explored. As shown in Fig. 2A, the FRET fluorescence intensity is linearly ($R^2 = 0.9597$) correlated to the undissolved C6/M NCs in the methanol/water binary systems, and this linear correlation was also found in FaSSIF and FeSSIF (Fig. S4).

#### 3.3.2. Reprecipitation study

Moreover, the reprecipitation study was conducted to study whether the FRET signal could be reilluminated after FRET pairs were released, because the released FRET pairs were proved to regenerate the FRET

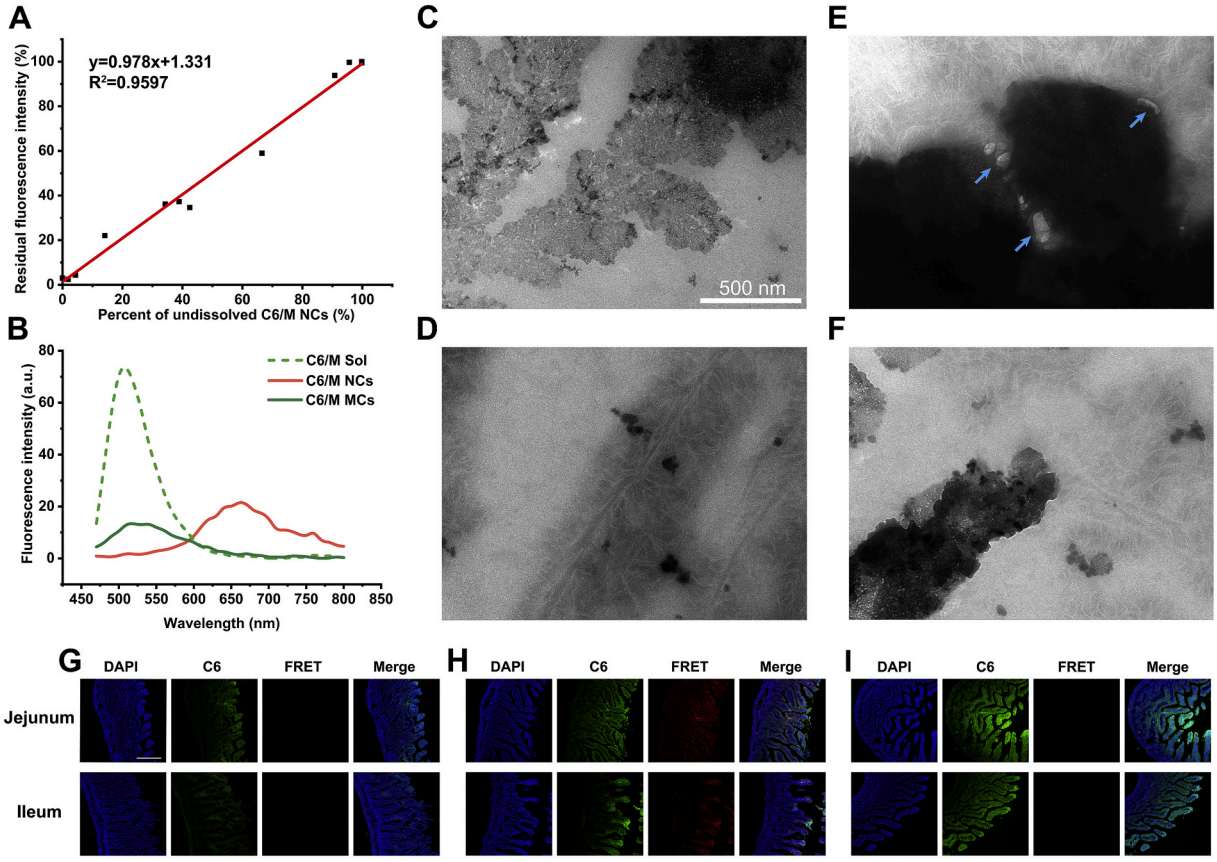


**Fig. 2.** (A) Linear correlation between undissolved C6/M NCs and fluorescence intensity in different water/methanol (*v/v*) binary systems. (B) Emission spectra of the samples on the basolateral side after transport *via* the mucus layer for C6/M MCs, C6/M NCs, and C6/M Sol. TEM images of the samples on the basolateral side after transport *via* the mucus layer for (C) the blank medium, (D) C6/M MCs, (E) C6/M NCs, and (F) C6/M Sol. Bule arrows indicate C6/M NCs. CLSM images of the frozen sections of intestinal loops after *in situ* absorption of (G) C6/M MCs, (H) C6/M NCs, and (I) C6/M Sol.

signal and interfere with the tracking of drug nanocarriers in previous studies [15,20,21]. As shown in Fig. S5, the FRET signal is not found in the reprecipitated C6/M NCs, indicating that no pseudo-signals are produced. The FRET signal is thus reliable for tracking C6 NCs accurately by embedding MeTTMN and constructing C6/M NCs.

### 3.3.3. Mucus permeation

The stability of the NCs was evaluated by measuring the particle sizes and FRET ratios. As shown in Table S1, during incubation for 24 h, both C6 NCs and C6/M NCs do not increase in sizes, and the FRET ratio of the diluted C6/M NCs shows no considerable change, indicating good dilution stability.

Mucus permeation was then performed to explore whether C6 and C6/M NCs could be tracked after passing through the mucus. The fluorescence spectra of the samples on the basolateral side were recorded. As shown in Fig. 2B, both the C6/M Sol and C6/M MC groups exhibited a specific emission between 500 and 550 nm, suggesting that the two formulations were permeated as free C6. In case of the C6/M NC group, an emission peak was found at approximately 650 nm, indicating that the NCs particles successfully penetrated the mucus. To confirm the results above, the samples collected on the basolateral side were directly visualized using the TEM (Fig. 2C–F). Rod-shaped nanoparticles were only observed in Fig. 2E, confirming that C6/M NCs particles passed through the mucus layer, while C6 penetrates the mucus layer in a molecular state for C6/M Sol and C6/M MC. The TEM images proved that both free C6 and C6/M NCs could be tracked by fluorescence signals after passing through the mucus layer.

### 3.3.4. In situ intestinal absorption

To further test the feasibility for tracking dissolved C6 and C6/M NCs under physiologic conditions, *in situ* intestinal absorption studies were conducted. For C6/M MCs (Fig. 2G) and C6/M Sol (Fig. 2I), only an apparent donor signal was observed in the intestine villi. In case of C6/M NCs (Fig. 2H), the coexistence of the donor signal and the FRET signal indicated that free C6 and C6/M NCs particles could be tracked simultaneously, confirming the reliability of this method.

## 3.4. In vitro dissolution

Biomimetic media can simulate intestinal fluids, and thus dissolution testing in biomimetic media is commonly performed to yield meaningful results [22]. In this study, dissolution test was performed in both FaSSIF and FeSSIF. As shown in Fig. 3, the incorporation of MeTTMN did not affect the dissolution rate of C6 NCs, as evidenced by the similar dissolution profiles for C6/M NCs and the physical mixture of C6 NCs and M NCs. The interference of MeTTMN in drug dissolution was thus precluded. In addition, the dissolved C6 from C6/M NCs was significantly higher than that from C6/M MCs both in FaSSIF ($p < 0.0001$) and FeSSIF ($p < 0.05$), indicating that nanocrystallization could lead to the dissolution improvement which might further contribute to oral absorption enhancement.

## 3.5. Gastrointestinal traffic and biodistribution

To understand how the NCs improved oral bioavailability, the gastrointestinal traffic of C6/M NCs was studied in mice by observing the fluorescence intensity after single-dose intragastric administration.

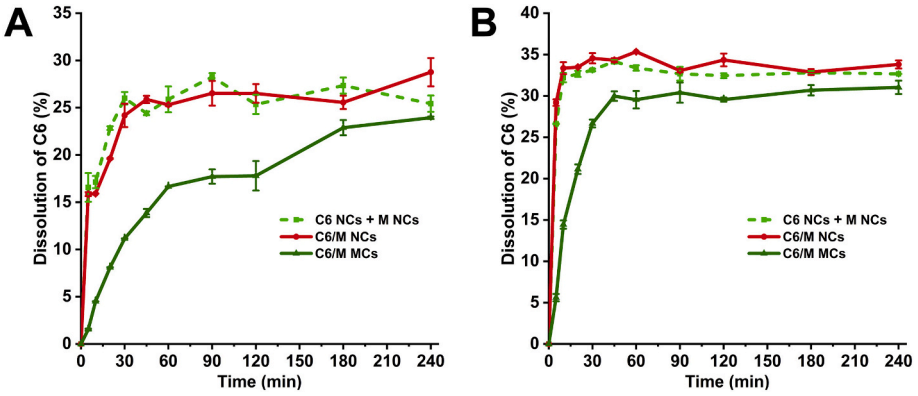


**Fig. 3.** The dissolution profiles of C6/M MCs, C6/M NCs, and the mixture of C6 NCs and M NCs in (A) FaSSIF and (B) FeSSIF.

The results are shown in Fig. 4A. Generally, the fluorescence signals were transferred from the stomach to the distal colon, which was caused by gastric emptying and intestinal motility. For the C6/M Sol group, only the donor signal was observed, but it gradually weakened from 0.05 to 12 h because of the absorption of free C6. For the C6/M NCs, both the donor and the FRET signals were observed, and the donor signal increased within 2 h while the FRET signal decreased gradually, indicating the dissolution of the NCs. Moreover, the donor signal weakened gradually after 2 h because of the intestinal absorption of free C6. For the C6/M MCs group, similar results were obtained, but the FRET signal disappeared at 6 h because of its slow dissolution rate.

The frozen sections of the isolated gastrointestinal tracts further revealed the absorption processes. For C6/M Sol (Fig. S6) and C6/M MCs (Fig. S7), only the donor signal was observed in the epithelial cells, indicating that Sol and MCs were absorbed in a molecular state for *in situ* studies. In case of the C6/M NCs group (Fig. 4B-E), both the donor and

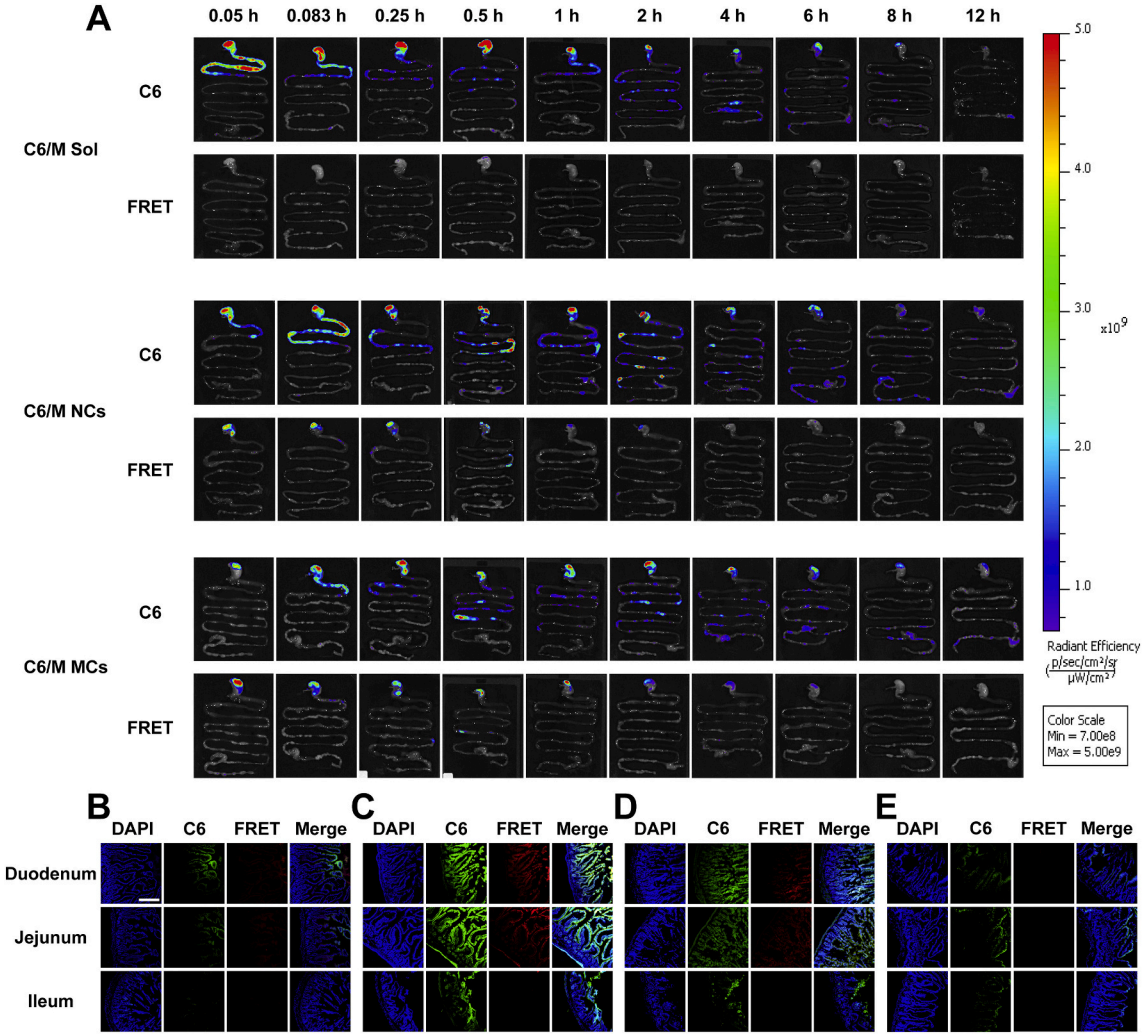


**Fig. 4.** (A) *Ex vivo* live imaging of whole gastrointestinal tracts. CLSM images of the frozen sections of mice intestinal loops after gavage administration of C6/M NCs at (B) 0.083, (C) 1, (D) 4, and (E) 8 h.

the FRET signals were observed in the epithelial cells, confirming that the NCs were absorbed as free molecules and NCs particles simultaneously. Specifically, both the signals were already observed at 0.083 h (Fig. 4B). From 0.083 to 1 h, their intensity was increased dramatically, indicating the simultaneously quick uptake of both free C6 and NCs particles by enterocytes. By contrast, from 1 to 8 h, both signals decreased (Fig. 4D-E), suggesting that the drug was gradually absorbed and distributed. In addition, an interesting finding for the *in-situ* study is that the donor signal was stronger and kept for a longer period than the FRET signal, indicating that a free molecule was the main absorption form for C6/M NCs. Weak FRET signals observed in the epithelial cells indicated endocytosis was involved in the oral absorption of C6 NCs, however, its contribution is very limited. Although previous studies stressed that nanoparticles were absorbed mainly by endocytosis, these conclusions were supported by data obtained from cellular studies, whose culturing volume was very limited, and thus the dissolution behaviors of the nanoparticles were ignored and endocytosis in absorption was exaggerated. However, for animal studies, a formulation is first dissolved and then be absorbed, and the dissolution is thus extremely important. Although the NCs in FaSSIF/FeSSIF were not completely dissolved *in vitro*, only weak FRET signals were observed in intestinal sections and limited endocytosis contributed to the absorption because of the interplay of dissolution and permeability *in situ* and *in vivo*. Recently, to better reflect the interplay of dissolution and permeability, dynamic dissolution/permeation tests [22] and *in situ* dissolution and permeation studies [23] were carried out, they work as valuable tools to promote mechanistic understanding during formulation development despite of limitation of experimental set-up.

The biodistribution of C6/M NCs was subsequently evaluated by observing the fluorescence signals in plasma and organs. *Ex vivo* live imaging of plasma was shown in Fig. 5A, and only the donor signal was found in all groups, indicating that C6 was in a molecular state in the blood. C6/M Sol showed the fastest absorption rate, which could be attributed to the fact that it does not require a dissolution process. In addition, C6/M NCs showed faster blood penetration rate than C6/M MCs because of their rapid dissolution.

For isolated organs, only the donor signal was found for all formulations (Fig. 5B). Specifically, despite some C6/M NCs were absorbed as particles, the FRET signal was not detected in any organ because C6 and MeTTMN were already dissolved and separated in the blood before distribution. In case of the donor signal, it was observed obviously in the liver and the kidney because C6 was primarily metabolized by the liver and excreted by the kidney [24]. In addition, the increase in the donor signal from 0.05 to 0.5 h indicated the accumulation of free C6, but the donor signal then gradually weakened from 0.5 h because of the metabolism and excretion of C6. The time-dependent donor signal was also observed in the C6/M Sol and C6/M MC groups.

In case of C6/M NCs, they can be absorbed either as a molecular form

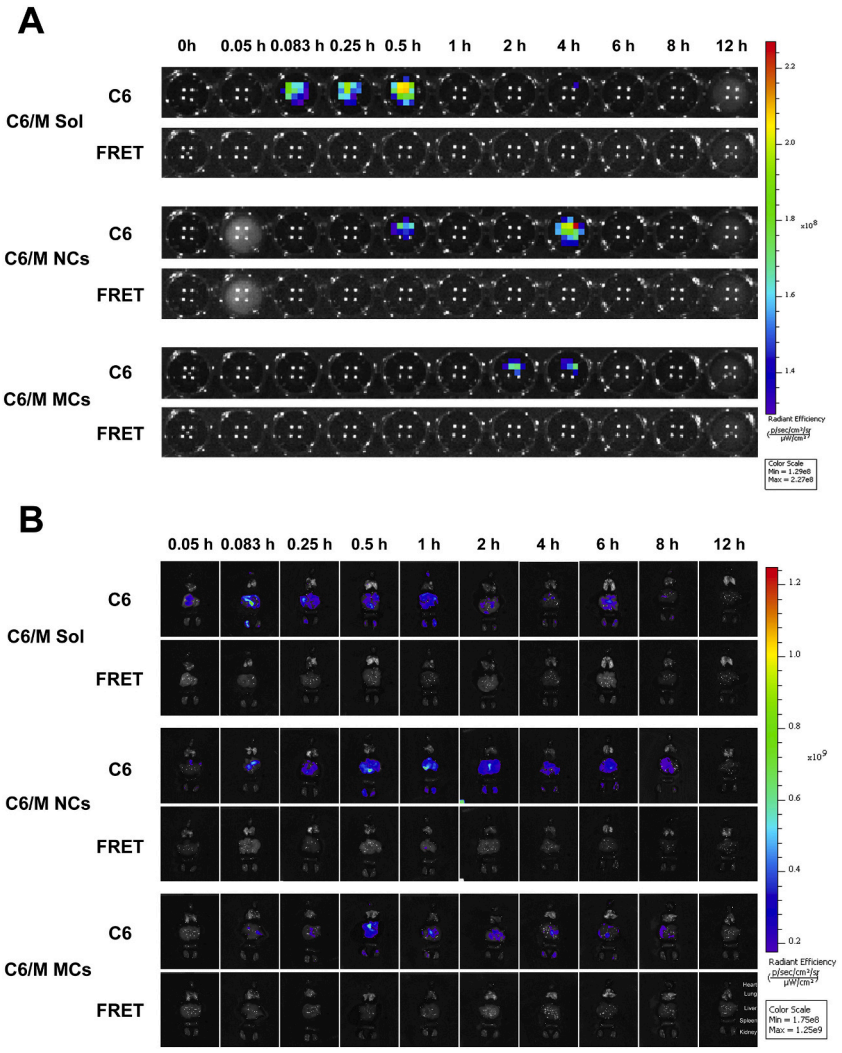


**Fig. 5.** *Ex vivo* live imaging of (A) plasma and (B) main organs (heart, lung, liver, spleen, and kidney, from top to bottom) after gavage administration of C6/M MCs, C6/M NCs, and C6/M Sol.

or as NCs particles as described above. However, the free C6 dominated absorption in the animal studies, suggesting that the drug NCs improved the drug performance *in vivo* mainly by increasing the dissolution. The improved solubility/dissolution is an important factor associated with oral absorption enhancement of formulations [23]. For poorly water-soluble drugs, dissolution acts as one of the rate-controlling steps and determines the rate and degree of absorption. Generally, the bioavailability of a drug can be improved by increasing its dissolution rate. However, the enhanced dissolution rate does not always significantly increase the absorption [25], because the drug must pass through the gastrointestinal tract before absorption. Thus, intestinal permeability is another key factor in oral absorption [25], and there are many ways for drugs to pass through epithelial cells, such as molecular diffusion and endocytosis. The dissolution and absorption (permeability) mutually affected each other. On one hand, the dissolution rate may affect the form of nanoparticles in the gastrointestinal tract and the way of drug penetrating membrane. Fast-dissolution drugs are more likely to be absorbed by diffusion. On the other hand, the absorption rate of a drug may also affect its dissolution. For drugs with good membrane permeability, the dissolved drugs will be quickly absorbed after oral administration, and the drugs can thus be continuously dissolved from the NCs particles, and *vice versa*. Thus, the interplay between dissolution and permeability plays an important role in oral absorption. In addition, besides solubility/permeability of a drug, considerations of particle sizes, crystal forms, morphologies, and *etc.* were also necessary. For example, 200 nm C6 NCs accumulated in lysosomes for digestion, while 70 nm C6 NCs accumulated in ER and lysosome for transport mediated by ER/Golgi and Golgi/PM pathways [26]. Though, for the convenience of tracing, C6 (an ACQ dye) was selected as the model drug in this article, this discovery is still of great significance for the application of NCs technology to improve the drugability of insoluble drugs.

## 4. Conclusion

In this study, to explore the absorption mechanism of NCs, MeTTMN was used to label C6 NCs. Thus, NCs particles and dissolved C6 were simultaneously tracked. The apparent donor signal in the intestines suggested that C6 was mainly absorbed in a molecular state *in vivo*, which was further supported by biodistribution results. This study suggested that the NCs improved oral bioavailability mainly by increasing dissolution for poorly water-soluble drugs. This finding bears significance for the wide application of drug NCs in improving the druggability of insoluble drugs.

## Acknowledgments

This work was financially supported by the National Science and Technology Major Project (No. 2017ZX09101001), by the National Nature Science Foundation of China (No. 81502993), by the Nature Science Foundation of Liaoning Province, by the Basic Research Projects of Universities of Liaoning Provincial Department of Education, and the Career Development Program for Young Teachers in Shenyang Pharmaceutical University (ZQN2019003).

## Appendix A. Supplementary data

Supplementary data to this article can be found online at https://doi.org/10.1016/j.jconrel.2021.02.025.

## References

[1] P. Boisseau, B. Loubaton, Nanomedicine, nanotechnology in medicine, Comp. Rend. Phys. 12 (2011) 620–636.
[3] B. Wahlang, Y.B. Pawar, A.K. Bansal, Identification of permeability-related hurdles in oral delivery of curcumin using the Caco-2 cell model, Eur. J. Pharm. Biopharm. 77 (2011) 275–282.
[4] F. Ahmad, A.K. Pandey, A.B. Herzog, J.B. Rose, C.P. Gerba, S.A. Hashsham, Environmental applications and potential health implications of quantum dots, J. Nanopart. Res. 14 (2012) 1038.
[5] H. He, Y. Xie, Y. Lv, J. Qi, X. Dong, W. Zhao, W. Wu, Y. Lu, Bioimaging of intact polycaprolactone nanoparticles using aggregation-caused quenching probes: size-dependent translocation via oral delivery, Adv. Healthc. Mater. 7 (2018) 1800711.
[6] J. Luo, Z. Xie, J.W.Y. Lam, L. Cheng, H. Chen, C. Qiu, H.S. Kwok, X. Zhan, Y. Liu, D. Zhu, B.Z. Tang, Aggregation-induced emission of 1-methyl-1,2,3,4,5-pentaphenylsilole, Chem. Commun. (2001) 1740.
[7] J. Qi, X. Hu, X. Dong, Y. Lu, H. Lu, W. Zhao, W. Wu, Towards more accurate bioimaging of drug nanocarriers: turning aggregation-caused quenching into a useful tool, Adv. Drug Deliv. Rev. 143 (2019) 206.
[8] T. Wang, J. Qi, N. Ding, X. Dong, W. Zhao, Y. Lu, C. Wang, W. Wu, Tracking translocation of self-discriminating curcumin hybrid nanocrystals following intravenous delivery, Int. J. Pharm. 546 (2018) 10–19.
[9] Y. Wang, Y. Zhang, J. Wang, X.J. Liang, Aggregation-induced emission (AIE) fluorophores as imaging tools to trace the biological fate of nano-based drug delivery systems, Adv. Drug Deliv. Rev. 143 (2019) 161–176.
[10] Y. Hong, J.W.Y. Lam, B.Z. Tang, Aggregation-induced emission: phenomenon, mechanism and applications, Chem. Commun. (2009) 4332–4353.
[11] Y. Chen, T. Li, Cellular uptake mechanism of paclitaxel nanocrystals determined by confocal imaging and kinetic measurement, AAPS J. 17 (2015) 1126–1134.
[12] Y. Lu, Y. Lv, T. Li, Hybrid drug nanocrystals, Adv. Drug Deliv. Rev. 143 (2019) 115–133.
[13] X. Zhang, Y. Hu, X. Yang, Y. Tang, S. Han, A. Kang, H. Deng, Y. Chi, D. Zhu, Y. Lu, FOrster resonance energy transfer (FRET)-based biosensors for biological applications, Biosens. Bioelectron. 138 (2019) 111314.
[14] S. Xiong, W. Liu, D. Li, X. Chen, F. Liu, D. Yuan, H. Pan, Q. Wang, S. Fang, T. Chen, Oral delivery of puerarin nanocrystals to improve brain accumulation and anti-Parkinsonian efficacy, Mol. Pharm. 16 (2019) 1444–1455.
[15] X. Lv, S. Zhang, H. Ma, P. Dong, X. Ma, M. Xu, Y. Tian, Z. Tang, J. Peng, H. Chen, J. Zhang, In situ monitoring of the structural change of microemulsions in simulated gastrointestinal conditions by SAXS and FRET, Acta Pharm. Sin. B 8 (2018) 655–665.
[16] K.R. Lee, I.J. Kang, Effects of dopamine concentration on energy transfer between dendrimer-QD and dye-labeled antibody, Ultramicroscopy 109 (2009) 894–898.
[17] M. Guo, M. Wei, W. Li, M. Guo, C. Guo, M. Ma, Y. Wang, Z. Yang, M. Li, Q. Fu, L. Yang, Z. He, Impacts of particle shapes on the oral delivery of drug nanocrystals: mucus permeation, transepithelial transport and bioavailability, J. Control. Release 307 (2019) 64–75.
[18] H. Chen, H.L. Puhl, S.V. Koushik, S.S. Vogel, S.R. Ikeda, Measurement of FRET efficiency and ratio of donor to acceptor concentration in living cells, Biophys. J. 91 (2006) L39–L41.
[19] X. Ma, R. Sun, J. Cheng, J. Liu, F. Gou, H. Xiang, X. Zhou, Fluorescence aggregation-caused quenching versus aggregation-induced emission: a visual teaching technology for undergraduate chemistry students, J. Chem. Educ. 93 (2016) 345–350.
[20] S.-Y. Lee, J.Y. Tyler, S. Kim, K. Park, J.-X. Cheng, FRET imaging reveals different cellular entry routes of self-assembled and disulfide bonded polymeric micelles, Mol. Pharm. 10 (2013) 3497–3506.
[21] H. Chen, S. Kim, L. Li, S. Wang, K. Park, J.-X. Cheng, Release of hydrophobic molecules from polymer micelles into cell membranes revealed by Förster resonance energy transfer imaging, Proc. Natl. Acad. Sci. 105 (2008) 6596.
[22] D. Sironi, J. Rosenberg, A. Bauer-Brandl, M. Brandl, Dynamic dissolution-/permeation-testing of nano- and microparticle formulations of fenofibrate, Eur. J. Pharm. Sci. 96 (2017) 20–27.
[23] M. Imono, H. Uchiyama, H. Ueda, K. Kadota, Y. Tozuka, In-situ dissolution and permeation studies of nanocrystal formulations with second-derivative UV spectroscopy, Int. J. Pharm. 558 (2019) 242–249.
[24] S.P. Felter, J.D. Vassallo, B.D. Carlton, G.P. Daston, A safety assessment of coumarin taking into account species-specificity of toxicokinetics, Food Chem. Toxicol. 44 (2006) 462–475.
[25] A. Dahan, J.M. Miller, The solubility-permeability interplay and its implications in formulation design and development for poorly soluble drugs, AAPS J. 14 (2012) 244–251.
[26] X.Q. Miao, Y. Li, X.Q. Wang, S.M.Y. Lee, Y. Zheng, Transport mechanism of coumarin 6 nanocrystals with two particle sizes in MDCKII monolayer and larval Zebrafish, ACS Appl. Mater. Interfaces 8 (2016) 12620–12630.
[27] C.P. Hollis, H.L. Weiss, M. Leggas, et al., Biodistribution and bioimaging studies of hybrid paclitaxel nanocrystals: lessons learned of the EPR effect and image-guided drug delivery, J. Control. Release 172 (2013) 12–21.